A Study of TDMR Signal Processing Opportunities Based on Quasi-Micromagnetic Simulations

Bane Vasić[1], Mehrdad Khatami[1], Yasuaki Nakamura[2], Yoshihiro Okamoto[2], Yasushi Kanai[3], John R. Barry[4], Steven W. McLaughlin[4], and Elnaz Banan Sadeghian[4]

[1]Department of Electrical and Computer Engineering, University of Arizona, Tucson, AZ 85721 USA
[2]Graduate School of Science and Engineering, Ehime University, Matsuyama 790-8577, Japan
[3]Department of Information and Electronics Engineering, Niigata Institute of Technology, Kashiwazaki 945-1195, Japan
[4]School of Electrical and Computer Engineering, Georgia Institute of Technology, Atlanta, GA 30332 USA

This paper presents the results of a comprehensive study of the shingled writing process and various signal processing and data detection approaches applied to the readback waveforms. The recording simulations include realistic head fields, a random granular media, magnetostatic and exchange interactions, and a READ head sensitivity function. Readback waveforms are examined in both one and two dimensions in terms of signal characteristics (linear and nonlinear), noise behavior (stationary and signal-dependent), and intertrack interference. Different equalization and detection approaches are compared and about a 10% density gain is reported for such 2-D magnetic recording compared with traditional single-track recording. These gains depend strongly on the number of readers, the reader positioning, and the reader width.

***Index Terms*— 2-D magnetic recording (TDMR), data-dependent noise, intersymbol interference (ISI), multitrack equalization and detection, shingled magnetic recording.**

I. Introduction

CONVENTIONAL magnetic recording has reached a point where the data storage densities cannot be increased due to energy stability constraints, and among new technologies, 2-D magnetic recording (TDMR) [1] is a promising approach to reach areal densities up to 10 Tb/in^2. A key component of TDMR is aggressive shingled writing [1], which enables narrow track widths comparable with the grain diameter by allowing each sweep of the WRITE head to partially overlap and overwrite previously written adjacent tracks. Evidently, this creates challenges including severe 2-D intersymbol interference (ISI), noise data dependence, and channel nonlinearity. In this paper, we address a broad range of technical challenges associated with TDMR modeling and detection and propose some solutions to mitigate the above effects. In particular, we consider a TDMR read/write channel all the components of which, including recording medium as well as write and readback processes, are realistically modeled in software. For such a channel, we investigate advanced data detection and synchronization techniques and their potential to increase data densities.

Recently, several read-channel models [2]–[7] based on the Voronoi model were proposed. In these models, each Voronoi region represents a magnetic grain. In [3]–[7], generating Voronoi regions is done by shifting the grain centers randomly from the cell centers. If the variance of the shift from cell centers is small, the randomness of the grain shape and position is unrealistically small. On the other hand, large deviation in grain centers leads to excessive increase in grain size dispersion. Yamashita *et al.* [8] used the Poisson disk distribution and Lloyd's relaxation method for the position of the grain centers. This model generates more realistic randomness and grain size dispersion. Furthermore, nonmagnetic grain boundaries are realized by applying a convex hull trimming [9] to the Voronoi cells iteratively. Yamashita *et al.* [7] proposed a simple write process considering magnetic clusters due to coupling between grains [10]. The write process is based on the Voronoi model with regard to magnetic clustering, WRITE head field gradient, media switching field distribution, and media switching field angle given by the Stoner–Wohlfarth (S–W) reversal mechanism. The writer having a triangular main-pole, a trailing-shield and a shield on one side of the pole [11] is employed. However, the write process does not include intergranular exchange fields and magnetostatic interaction fields between grains. In this paper, a modified write process is used in order that magnetic clusters are naturally formed by including these fields [8]. The reader output is generated via the 2-D convolution of the magnetization and the reader sensitivity function. The writing and readback timings are assumed to be perfect. The reading process is modeled by a double-shielded reader sensitivity function [6], which is obtained by fitting to sensitivity function generated from the 2-D-finite element method (FEM) for different head and medium geometries based on a calculation method that appeared in [12].

As noted in [4], in contrast to conventional recording systems, the primary source of noise in TDMR comes from the irregular boundaries of grains and the lack of knowledge of these boundaries during the readback process. Moreover, such noise is correlated and data-dependent. In this paper, we analyze the data-dependent noise characteristic of the readback signal generated by the media model discussed above. To compensate the SNR loss due to a decrease in the bit area, we assess the gains from the use of multiple readers in

Manuscript received July 18, 2014; accepted August 30, 2014. Date of current version May 18, 2015. Corresponding author: B. Vasić (e-mail: vasic@ece.arizona.edu).

Color versions of one or more of the figures in this paper are available online at http://ieeexplore.ieee.org.

Digital Object Identifier 10.1109/TMAG.2014.2356455

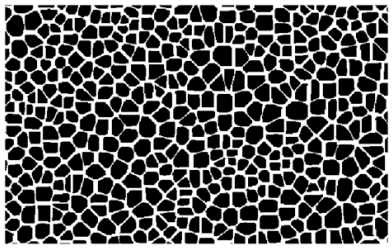

Fig. 1. Discretized granular medium model ($\langle\phi\rangle = 5.0$ nm, $\sigma_\phi/\langle\phi\rangle = 0.20$, and $\langle a\rangle = 1.0$ nm).

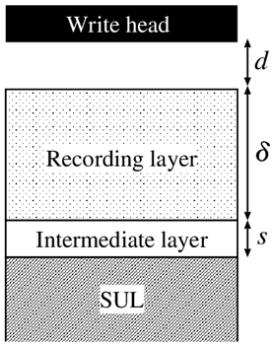

Fig. 2. Cross section of the head media geometry ($d = 4$ nm, $\delta = 10$ nm, and $s = 1$ nm).

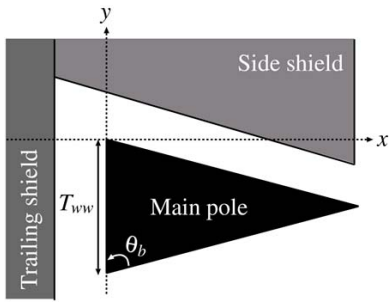

Fig. 3. Structure of triangular writer ($T_{ww} = 50$ nm, and $\theta_b = 75°$).

the TDMR system. We implemented several detection schemes used in the literature. This paper considers the application of BCJR detectors with 1-D and 2-D targets for our read channel. Since the primary source of noise in TDMR arises from irregularities in the recording medium and leads to highly colored and data-dependent noise, pattern-dependent noise predictive (PDNP) detection [13], [14] is also implemented to improve the performance. To compute the gains of using two readers, the symmetric information rate (SIR) can be computed as a measure of the achievable storage densities. In [15], the SIR for binary-input channels with memory is computed by standard forward sum-product (BCJR) processing of the simulated channel output. Here, we embedded the PDNP algorithm in the forward BCJR algorithm to compute a more accurate approximation of the SIR for one and two reader systems.

Traditional track-based recording systems employ separate strategies for synchronization in the two dimensions. Typically, servo signals and an active control loop are used for synchronization in the cross-track direction while using data-aided timing recovery in the down-track direction. However, moving to TDMR with multiple readers will merge these two problems into one: that of determining the precise position of each recorded bit in the face of writing and reading cross-track position errors (misregistration), grain effects, and mismatches in the local oscillator and disk rotation speed. The use of multiple readers enables the mitigation of cross-track errors via signal processing after sampling, relaxing the alignment requirements of the real-time position control system. A 2-D phase-locked loop has been proposed to solve such a synchronization problem for the case of a linear additive white Gaussian noise (AWGN) channel with a separable impulse response [16]. In this paper, we show that linear suppression of interference from neighboring tracks can be accomplished asynchronously using a traditional 1-D synchronization loop.

This paper is organized as follows. Section II introduces the read channel model in detail. In Section III-A, the data-dependent characteristic of the noise is described. The performances of multireader detectors are compared for our model in Section III-B. The SIR estimation of the channel is provided in Section III-C. Section IV explains the strategies for synchronization in TDMR. Finally, Section V concludes this paper.

II. Read/Write Modeling and Simulations

We assume discretized granular media with nonmagnetic grain boundaries based on a discrete Voronoi model introduced in [6]. Fig. 1 shows an example of the discrete granular medium model. The black polygons and white gaps show the magnetic grains and nonmagnetic grain boundaries, where the average grain size, the grain size dispersion normalized by the average grain size, and the average nonmagnetic grain boundary are set to $\langle\phi\rangle = 5.0$ nm, $\sigma_\phi/\langle\phi\rangle = 0.20$, and $\langle a\rangle = 1.0$ nm, respectively. The cross section of the head-medium geometry is shown in Fig. 2, where the head-medium spacing, the thickness of the granular layer, and the thickness of the intermediate layer in the medium are set to $d = 4$ nm, $\delta = 10$ nm, and $s = 1$ nm, respectively. In Fig. 3, the writer has a triangular main-pole, a trailing-shield, and a shield on one side of the pole [11]. The physical write track width and the base angle of the main-pole are set to $T_{ww} = 50$ nm and $\theta_b = 75°$, respectively. The write field intensity and angle are calculated by the FEM [11] and are shown in Fig. 4(a) and (b). The angle formed by the WRITE head field and the axis perpendicular to the medium plane is denoted by θ_{angle}. In the figures, the triangle shows the footprint of the main-pole. The effective WRITE head field H_{eff} is defined by $H_{\text{eff}} = H_w H_k / H_{\text{sw}}$. Here, H_k is the anisotropy field and H_{sw} is the switching field based on the S–W reversal mechanism according to the ψ_{angle} and θ_{angle}. Here, ψ_{angle} stands for the angle formed by the anisotropy axis of each grain and the perpendicular axis, and the angle is assumed to be 0° [10]. The switching field based on the S–W reversal mechanism is given by the following:

$$H_{\text{sw}} = H_k(\sin(\theta_{\text{angle}} + \psi_{\text{angle}})^{2/3} + \cos(\theta_{\text{angle}} + \psi_{\text{angle}})^{2/3})^{-3/2}. \quad (1)$$

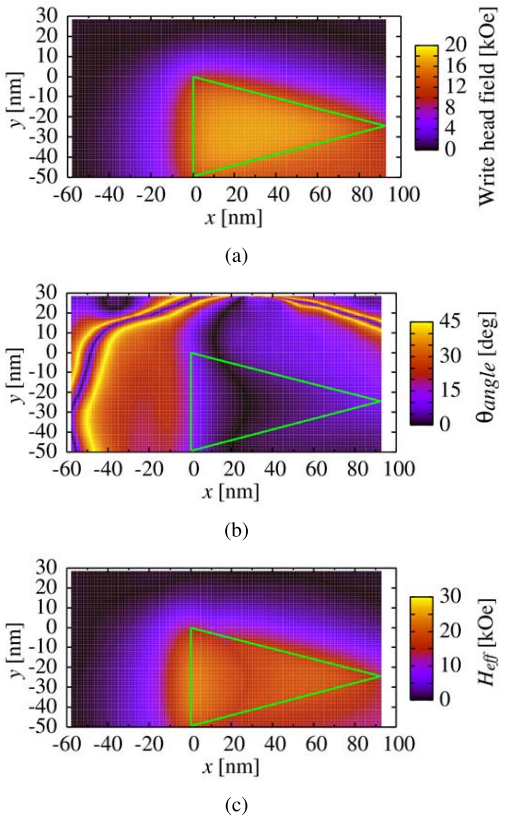

Fig. 4. (a) WRITE head field intensity. (b) WRITE head field angle. (c) Effective WRITE head field intensity.

We show the effective WRITE head field in Fig. 4(c). The field around the center of the trailing edge is strong and weakens with distance from the edge. The magnetization switching is determined by comparing the total applied field with saturation field of each grain. The condition to switch the magnetization direction of grain i on the medium by the writer is given by the following inequality:

$$H_{w,i}\ H_{d,i} + H_{\mathrm{ex},i} \geq H_{\mathrm{self},i} + H_{\mathrm{sw},i} \tag{2}$$

where $H_{w,i}$ is the WRITE head field from the writer at the centroid of grain i, $H_{d,i}$ is the magnetostatic interaction field which grain i experiences from other grains, $H_{\mathrm{ex},i}$ is the intergranular exchange field which grain i experiences from neighbors, $H_{\mathrm{self},i}$ is the self-demagnetizing field of grain i, and $H_{\mathrm{sw},i}$ is the switching field of grain i [10]. Fig. 5 shows an example of the shingle-written magnetization pattern on the discretized granular medium. The directions of axes x and y are called the down-track and cross-track directions, respectively. The channel bit length $l_c = 7.3$ nm and the track pitch $l_{\mathrm{tp}} = 22.1$ nm are assumed, and the dimensions correspond to an areal channel density of 4 Tb/in^2. The readers are assumed to be full-shielded as shown in Fig. 6. The width between side shields H, the shield gap G, the width T, and thickness U of magnetoresistive element of the reader are set to $H = 30$ nm, $G = 22$ nm, $T = 17$ nm, and $U = 2$ nm, respectively. Fig. 7 shows the reader sensitivity function obtained by a 2-D FEM [17]. We assume that the center of the main track is 0 nm and the reader moves

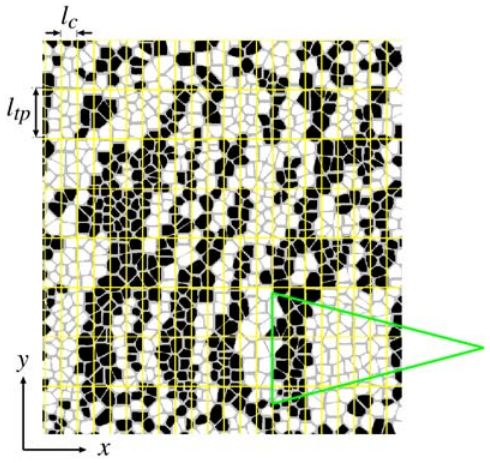

Fig. 5. Shingle-written magnetization pattern on the discretized granular medium ($l_c = 7.3$ nm and $l_{\mathrm{tp}} = 22.1$ nm).

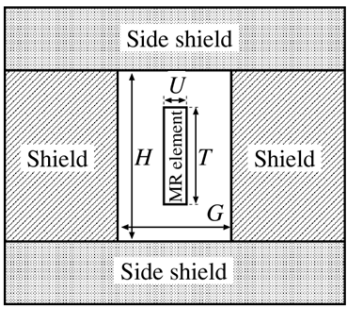

Fig. 6. Air bearing surface view of a fully shielded MR head. H, G, T, and U stand for the width between side shields, the shield gap, the width and thickness of magnetoresistive element of the reader, respectively.

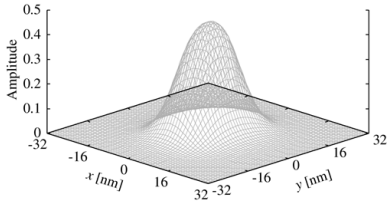

Fig. 7. Reader sensitivity function obtained using a 2-D FEM ($H = 30$ nm, $G = 22$ nm, $T = 17$ nm, and $U = 2$ nm).

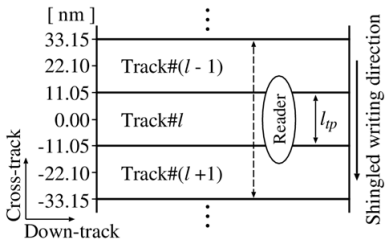

Fig. 8. Configuration of the reader and tracks.

from -33.15 to 33.15 nm on the main and adjacent tracks by an interval of $l_{\mathrm{tp}}/8$ as shown in Fig. 8. The reproducing waveforms from the granular media are obtained by convolution of the reader sensitivity function and medium magnetization as shown in Fig. 5.

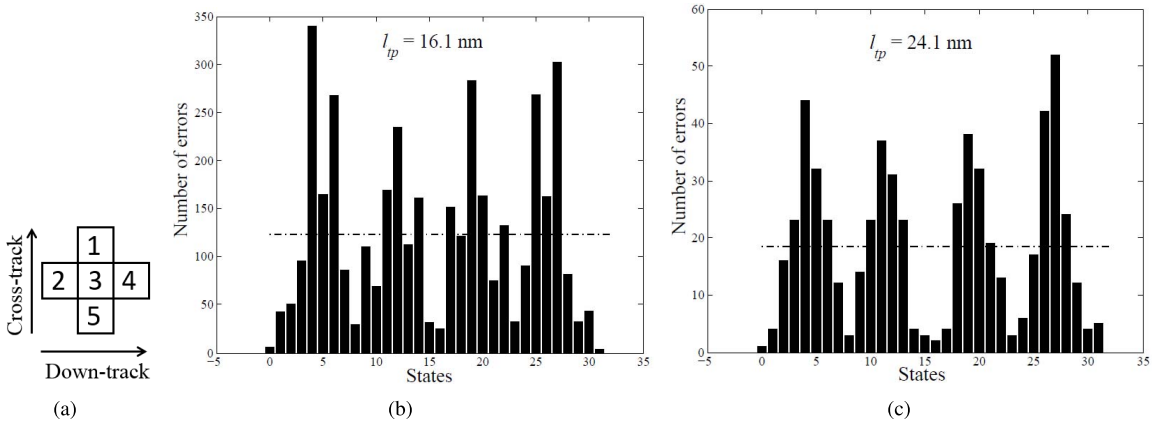

Fig. 9. (a) 2-D target used in noise analysis simulations. (b) Number of errors that occur for different input patterns for $l_{\text{tp}} = 16.1$ nm. (c) Number of errors that occur for different input patterns for $l_{\text{tp}} = 24.1$ nm.

Five consecutive shingled tracks were written on the medium, and readback waveforms were created at closely spaced read positions spanning three tracks in the center. This process was repeated for a series of l_{tp} decreasing from 34.0 to 16.1 nm track pitch. In the set of waveform generated for the simulations, the number of bits in the down-track dimension is 40 950. The results shown in the following sections are based on the simulation done on this set of waveforms.

III. Data-Dependent Noise and Multitrack Detectors

Data-dependent media noise and severe intertrack interference (ITI) are the two main challenges in TDMR systems, and must be mitigated by the detector [18]. We first consider the characteristics of the media noise in Section III-A, and then provide a performance comparison of various multitrack detectors in Section III-B. To provide more insights on the performance gain of the two reader TDMR system, we give the SIR estimation in Section III-C.

The equalizer used in the simulations for generating 1-D and 2-D targets is the generalized partial response (GPR) equalizer [19]. Let T be an $L_1 \times L_2$ matrix representing the GPR target of size $L_1 \times L_2$. The target is called 2-D where $L_1 > 1$; otherwise, the target is 1-D ($L_1 = 1$). Let F be an $R \times N$ matrix representing the equalizer filter coefficients where R denotes the number of readers and N denotes the equalizer filter taps in the down-track direction, which is set to $N = 15$ throughout this paper. The GPR objective is to find the target and the equalizer filter simultaneously by minimizing the mean squared error between the equalizer output and the desired signal, subject to a minimum-phase constraint on the target.

A. Noise Analysis

In this paper, we have equalized the channel to a GPR target with three taps in the down-track direction (1×3 target), which is then followed by a BCJR detector to compute the number of bit errors for different input patterns and different track pitches (l_{tp}) with an order of significant bits 1–5 is shown in Fig. 9(a). The 32 states shown in Fig. 9(b) and (c) are calculated by $s = \sum_{i=1}^{5} X_i 2^{X_i - 1}$, where $X_i \in \{0, 1\}$ is the value of the bit with the order of significance i shown in Fig. 9(a). Fig. 9(b) shows the number of errors for different input patterns in the form of Fig. 9(a) with 32 states. It is shown that for narrow track pitch ($l_{\text{tp}} = 16.1$ nm) which leads to severe ITI, the most harmful input patterns are the result of two consecutive transitions of input bits in the cross-track direction. Fig. 9(c) shows that for $l_{\text{tp}} = 24.1$ nm, the most harmful input patterns are the ones with two transitions in both cross- and down-track directions. To assess the harmfulness of different input patterns, Fig. 10(a) and (b) is provided. In the

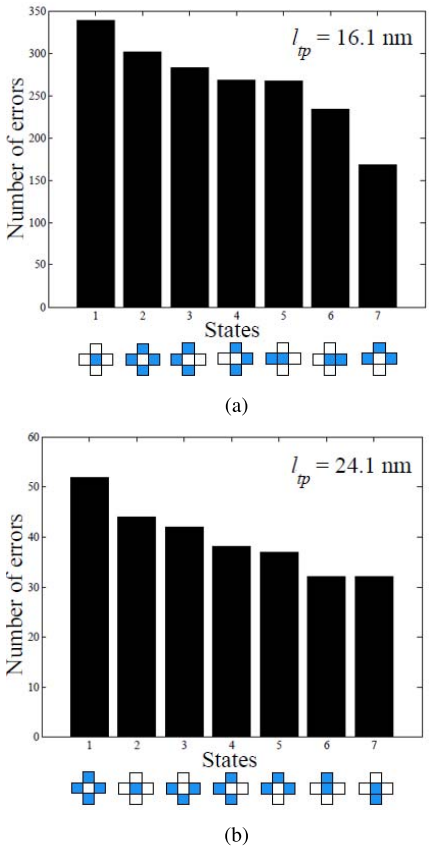

Fig. 10. Most harmful input patterns for (a) $l_{\text{tp}} = 16.1$ nm and (b) $l_{\text{tp}} = 24.1$ nm.

l_{tp} [nm]								
16.1	0.0571	0.1397	0.1887	0.1318	0.1265	0.1783	0.1168	0.0612
18.1	0.0428	0.1370	0.1884	0.1366	0.1362	0.1833	0.1257	0.0498
20.1	0.0325	0.1571	0.2116	0.1119	0.1043	0.1901	0.1513	0.0412
24.1	0.0186	0.1740	0.2145	0.0861	0.0676	0.2601	0.1520	0.0270
26.1	0.0169	0.1687	0.2145	0.1036	0.0819	0.2241	0.1590	0.0313
28	0.0122	0.1702	0.2432	0.0699	0.0517	0.2644	0.1550	0.0334
32	0.0133	0.1867	0.2222	0.0356	0.0533	0.2444	0.2044	0.0400
34	0.0156	0.2188	0.2396	0.0625	0.0312	0.2031	0.1771	0.0521

(a)

l_{tp} [nm]								
16.1	0.0391	0.1061	0.2547	0.1003	0.1011	0.2552	0.1067	0.0368
18.1	0.0471	0.1043	0.2320	0.1098	0.1144	0.2336	0.1102	0.0487
20.1	0.0493	0.1304	0.2232	0.0788	0.0777	0.2267	0.1588	0.0551
24.1	0.0726	0.1318	0.1723	0.1182	0.1284	0.1875	0.1233	0.0659
26.1	0.0771	0.1422	0.1542	0.1325	0.1301	0.1422	0.1422	0.0795
28	0.1064	0.1398	0.1337	0.1368	0.0973	0.1550	0.1307	0.1003
32	0.0978	0.1511	0.1156	0.1422	0.1644	0.0844	0.1244	0.1200
34	0.1198	0.1354	0.1250	0.1406	0.1042	0.1094	0.1302	0.1354

(b)

Fig. 11. Error percentage for all the cases of three consecutive bits in horizontal and vertical dimensions for different l_{tp} values.

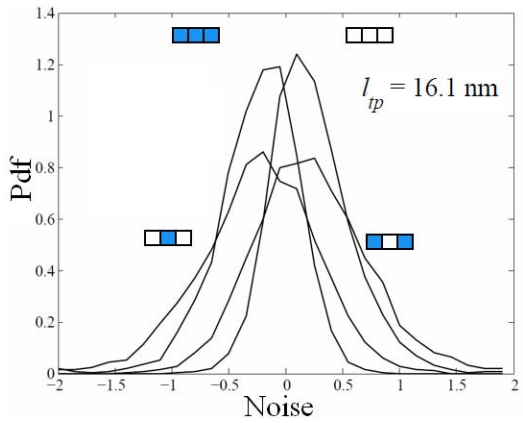

Fig. 12. PDFs of the noise for different input patterns for $l_{\text{tp}} = 16.1$ nm. The color blue is assigned for 1 and white is assigned for -1.

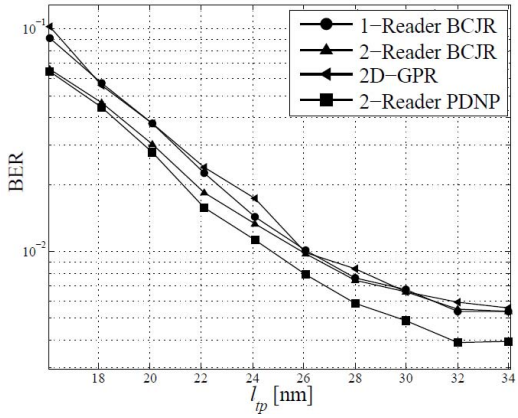

Fig. 13. BER comparison of the detection schemes for the TDMR model. 1) Conventional one-reader equalization and BCJR detector; 2) two-reader equalization with 1-D target and BCJR detector; 3) two-reader equalization with 2-D target and BCJR detector; and 4) two-reader equalization with 1-D target and PDNP detection.

remainder of this paper, 1/0 bits are colored as blue/white, respectively. Fig. 10(a) shows the most harmful patterns for $l_{\text{tp}} = 16.1$ nm, and Fig. 10(b) shows the most harmful patterns for $l_{\text{tp}} = 24.1$ nm. These figures show that by increasing the track pitch, the dependency of the media noise on the transition of input in cross-track dimension gradually fades away. As a result, the most harmful patterns for the readback signal of $l_{\text{tp}} = 34.0$ nm are the ones with two consecutive transitions in the down-track direction. Fig. 11(a) and (b) shows the number of errors for the conventional 1-D detection for all cases of three consecutive bits in horizontal and vertical dimensions. As it is shown, the number of errors for a narrower track pitch directly depends on the number of transitions in the cross-track dimension for narrower track pitch. As the track pitch increases, this dependency slowly fades away. For a constant bit-period, errors mostly occur when we have more transitions in the down-track dimension. Furthermore, the probability density function (pdf) of the media noise for different input patterns is provided in Fig. 12, which also shows the data-dependent characteristic of the media noise.

B. Detection Schemes

To determine the most appropriate detection strategy for multireader read channels, we have simulated and compared three detection schemes. For the two reader simulations, the multireader detector is designed such that the first reader is positioned at the center of the main track (0 nm) and the second reader is at the center of the upper adjacent track.

The first scheme uses a single reader and conventional 1-D equalization and detection. In this method, a single reader output is equalized to a three tap (1×3) 1-D target and the BCJR algorithm is employed for detection. The BCJR algorithm assumes the noise to be AWGN with the noise variance equal to the variance of the residual noise of the equalizer. In the second scheme, the samples from two readers are equalized to 1-D and 2-D targets, and the equalizer outputs are then sent to a BCJR algorithm for detection. In the last method, a PDNP detector [14] is used to benefit from the fact that the equalizer output noise is colored and data-dependent. By inserting a noise prediction/whitening process into the branch metric computation of the BCJR algorithm, the PDNP detector is constructed. The PDNP detector uses different noise prediction filters for different input patterns in the trellis of the BCJR detector to take advantage of the data dependency of the media noise. The computation of the coefficients of the noise predictors and pattern-dependent variances is performed by a linear MMSE predictor. Fig. 13 compares the detection schemes for the read channel model in terms of bit error rate (BER). Single-reader and two-reader equalizers with 1-D and 2-D targets are compared with and without PDNP detection.

C. SIR of Read Channel Model

To compute the density gains due to using multiple readers, the capacity of the channels for both cases must be

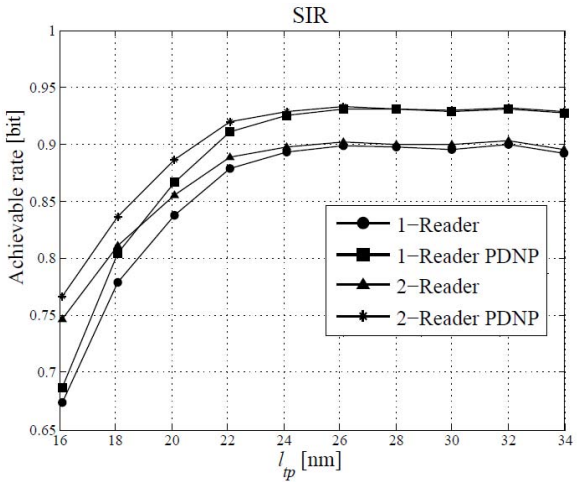

Fig. 14. SIR estimation of one and two reader scenarios. The PDNP algorithm is used to compute a better approximation of the SIR of the channel.

computed. A simpler problem than computing the capacity is the computation of the mutual information of the input X and the output Y, where X is binary and uniformly distributed. This mutual information is called SIR. The capacity and SIR can serve as performance benchmarks for channel coding and detection methods indicating the achievable storage densities.

The SIRs of one reader and two reader scenarios are compared in this section. Using GPR equalization, the output Y denotes the output samples of the equalizer in case of both one and two readers. In [15], the SIR for binary-input channels with memory is computed by standard forward sum-product (BCJR) processing of the simulated channel output. We can use a similar approach to approximate the SIR. Using 1-D target, the read channel can be estimated by 1-D ISI channel. To use the method in [15], the residual noise is approximated by AWGN with the same variance. The estimation of the SIR would be accurate if the residual noise of the equalizer is AWGN. To have a more accurate approximation of the SIR, we have used the PDNP method in the forward recursion of the BCJR algorithm. In other words, using the PDNP method, let us break the channel into separate small channels for different input patterns. By employing noise prediction/whitening filters, the AWGN approximation of the noise in the branch metric computation is better, which results in a more accurate SIR approximation.

Fig. 14 shows the estimation of SIR using the forward BCJR algorithm for the one and two reader cases. Furthermore, the PDNP algorithm is used to compute better approximation of the SIR for the ISI channel with data-dependent and colored noise.

IV. Joint Detection and Synchronization

While it is reasonable to consider multiple readers per slider, the most practical design for writing will have only a single WRITE head per slider. As a result, the bits on neighboring tracks will not be synchronized. There may furthermore be a frequency offset caused by variations in rotational speeds,

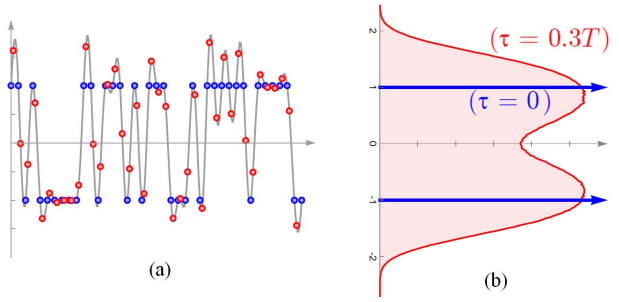

Fig. 15. Relationship between the written bits $a_k^{(n)}$ and their fractionally delayed counterparts $d_k^{(n)}$, when $\tau_n = 0.3T$.

causing neighboring tracks to have slightly different bit rates. A fundamental question arises: must we have knowledge of the timing offsets for the bits of an interfering track when mitigating its interference? Here, we demonstrate that the answer is no for the special case of linear ITI suppression and constant timing phase offsets; in this case, the ITI can be suppressed asynchronously (without any knowledge of its timing phase), so that a synchronization loop is needed only for the track or tracks of interest. A clear benefit is that synchronization is not needed for each analog-to-digital converter (ADC) (or equivalently each READ head); rather it is only needed for each detected track, and it can leverage existing and mature 1-D synchronization strategies.

Let $a_k^{(n)}$ denote the kth bit written on the nth track. If these bits modulated a minimum-bandwidth pulse shape and were sampled at the bit rate asynchronously with a timing offset of τ_n, the result would be $d_k^{(n)} = a_k^{(n)} * \mathrm{sinc}(k - \tau_n/T)$. The relationship between $a_k^{(n)}$ and $d_k^{(n)}$ is shown in Fig. 15. The blue samples in Fig. 15(a) represent $a_k^{(n)}$ after sampling synchronously, while the red samples represent $d_k^{(n)}$ after sampling asynchronously. The histograms in Fig. 15(b) show the stark difference between the two sequences. Nevertheless, somewhat unexpectedly, $a_k^{(n)}$ and $d_k^{(n)}$ have identical second-order statistics since

$$E\left(d_k^{(n)}\right) = 0, \quad E\left(d_k^{(n)} d_{k+m}^{(n)}\right) = \delta_m. \tag{3}$$

The value of τ_n has no impact on the mean and autocorrelation function.

Based on a linear model for the output of the ith reader ADC in the presence of a timing offset, the kth sample of the ith ADC output can be modeled as

$$r_k^{(i)} = \sum_n g_{i,n} x_k^{(n)} + n_k^{(i)} \tag{4}$$

where $x_k^{(n)} = d_k^{(n)} * h_k$ is the noise-free sequence from track n with timing offset τ_n, which results by convolving $d_k^{(n)}$ with the ISI response h_k, where $n_k{}^{(i)}$ are zero-mean white noise samples with variance σ^2, and where $g_{i,n}$ is the cross-track response gain from track n at READ head i. Collecting the N samples from each of the N READ heads at time k into the vector $\mathbf{r}_k = [r_k^{(1)}, \ldots r_k^{(N)}]^T$ leads to the vector model

$$\mathbf{r}_k = \sum_n x_k^{(n)} \mathbf{g}_n + \mathbf{n}_k \tag{5}$$

where $\mathbf{n}_k = [n_k^{(1)}, \ldots, n_k^{(N)}]^T$ is the noise vector and $\mathbf{g}_n = [g_{1,n}, \ldots, g_{N,n}]^T$ is the spatial ITI signature of the nth track.

In the case of linear ITI suppression (such as the two-reader detector with a 1-D target described in Section III-B), the weights that minimize the mean square error between the linear combiner output and the ITI-free samples (but with timing offset) of the ith track are

$$\mathbf{w}_i = \mathbf{R}^{-1}\mathbf{p} \tag{6}$$

where $\mathbf{R} = E(\mathbf{r}_k \mathbf{r}_k{}^T) = E_x \sum_n \mathbf{g}_n \mathbf{g}_n{}^T + \sigma^2 \mathbf{I}$ and $\mathbf{p} = E(x_k^{(i)} \mathbf{r}_k) = E_x \mathbf{g}_i$. These weights appear to depend on the timing offsets τ_n through the energy $E_x = E((x_k^{(n)})^2)$ of the ISI symbols $x_k^{(n)} = d_k^{(n)} * h_k$. However, the fact that the mean and autocorrelation of $d_k^{(n)}$ is independent of τ_n implies that E_x is independent of the timing offsets. The combining weights are thus independent of the timing phase of the interfering tracks, which means that ITI can be suppressed asynchronously before synchronization. These results extend to the case of a different frequency offset for each track: as long as the frequency offset is reasonably small, ITI can be linearly suppressed asynchronously with minimal penalty. A practical implication of this result is that a three-reader detector (for example) does not need three different synchronization loops, one for each reader; the equalizer coefficients will be invariant to the timing offsets of the interfering tracks. Only a single 1-D timing loop is needed after the equalizer and before the BCJR detector. Effective synchronization strategies for trellis-based detectors with 2-D targets can be devised based on per-survivor or per-node principles [20].

V. Conclusion

Our study suggests that a TDMR benefits from advanced signal processing, which unlike traditional single-track systems, operates on multiple data tracks. For example, at BER $= 10^{-2}$, a two-reader read channel combined with PDNP results in a 10% radial density increase. Future work includes developing 2-D modulation error correcting codes to reduce ISI and ITI, design of 2-D detectors based on generalized belief propagation algorithms as well as joint modulation and detection.

Acknowledgment

The authors would like to thank Prof. Muraoka and Associate Prof. S. Greaves of Tohoku University for their helpful discussions. This work was supported in part by the IDEMA-ASTC, the Storage Research Consortium, Japan, the Japan Society for the Promotion of Science under Grants-in-Aid for Young Scientists (B) 25820161 and Scientific Research (C) 26420358, and in part by the NSF under Grant CCF-1314147.

References

[1] R. Wood, M. Williams, A. Kavcic, and J. Miles, "The feasibility of magnetic recording at 10 terabits per square inch on conventional media," *IEEE Trans. Magn.*, vol. 45, no. 2, pp. 917–923, Feb. 2009.

[2] S. Mita, V. T. Van, and F. Haga, "Reduction of bit errors due to intertrack interference using LLRs of neighboring tracks," *IEEE Trans. Magn.*, vol. 47, no. 10, pp. 3316–3319, Oct. 2011.

[3] A. R. Krishnan, R. Radhakrishnan, B. Vasic, A. Kavcic, W. Ryan, and F. Erden, "2-D magnetic recording: Read channel modeling and detection," *IEEE Trans. Magn.*, vol. 45, no. 10, pp. 3830–3836, Oct. 2009.

[4] A. R. Krishnan, R. Radhakrishnan, and B. Vasic, "Read channel modeling for detection in two-dimensional magnetic recording systems," *IEEE Trans. Magn.*, vol. 45, no. 10, pp. 3679–3682, Oct. 2009.

[5] K. Sann Chan *et al.*, "TDMR platform simulations and experiments," *IEEE Trans. Magn.*, vol. 45, no. 10, pp. 3837–3843, Oct. 2009.

[6] M. Yamashita *et al.*, "Read/write channel modeling and two-dimensional neural network equalization for two-dimensional magnetic recording," *IEEE Trans. Magn.*, vol. 47, no. 10, pp. 3558–3561, Oct. 2011.

[7] M. Yamashita *et al.*, "A study on modeling of the writing process and two-dimensional neural network equalization for two-dimensional magnetic recording," *J. Appl. Phys.*, vol. 111, no. 7, pp. 07B727-1–07B727-3, Mar. 2012.

[8] M. Yamashita *et al.*, "Modeling of writing process for two-dimensional magnetic recording and performance evaluation of two-dimensional neural network equalizer," *IEEE Trans. Magn.*, vol. 48, no. 11, pp. 4586–4589, Nov. 2012.

[9] M. Igarashi, M. Hara, A. Nakamura, and Y. Sugita, "Micromagnetic simulation of magnetic cluster, thermal activation volume, and medium noise in perpendicular recording media," *IEEE Trans. Magn.*, vol. 39, no. 4, pp. 1897–1901, Jul. 2003.

[10] M. Yamashita, Y. Okamoto, Y. Nakamura, H. Osawa, S. J. Greaves, and H. Muraoka, "Performance evaluation of neuro-ITI canceller using a modified writing process for TDMR," *IEICE Trans. Electron.*, vol. E96-C, no. 12, pp. 1504–1507, Dec. 2013.

[11] Y. Kanai, Y. Jinbo, T. Tsukamoto, S. J. Greaves, K. Yoshida, and H. Muraoka, "Finite-element and micromagnetic modeling of write heads for shingled recording," *IEEE Trans. Magn.*, vol. 46, no. 3, pp. 715–721, Mar. 2010.

[12] Y. Suzuki, Y. Nishida, and H. Aoi, "Spacing loss factor for the read back from a perpendicular medium with a soft underlayer," *J. Mag. Mag. Mater.*, vol. 287, pp. 138–143, Feb. 2005.

[13] A. Kavcic and J. M. F. Moura, "The Viterbi algorithm and Markov noise memory," *IEEE Trans. Inf. Theory*, vol. 46, no. 1, pp. 291–301, Jan. 2000.

[14] J. Moon and J. Park, "Pattern-dependent noise prediction in signal-dependent noise," *IEEE J. Sel. Areas Commun.*, vol. 19, no. 4, pp. 730–743, Apr. 2001.

[15] D. Arnold and H.-A. Loeliger, "On the information rate of binary-input channels with memory," in *Proc. IEEE Int. Conf. Commun.*, vol. 9. Jun. 2001, pp. 2692–2695.

[16] K. M. Whelan, F. Balado, N. J. Hurley, and G. C. M. Silvestre, "A two-dimensional extension of the Mueller and Müller timing error detector," *IEEE Signal Process. Lett.*, vol. 14, no. 7, pp. 457–460, Jul. 2007.

[17] M. Yamashita *et al.*, "A study of read/write channel modeling for two-dimensional magnetic recording," *IEICE Tech. Rep.*, vol. 110, no. 329, pp. 31–38, Dec. 2010.

[18] S. M. Khatami and B. Vasic, "Detection for two-dimensional magnetic recording systems," *J. Commun.*, vol. 8, no. 4, pp. 233–239, Apr. 2013.

[19] J. Moon and W. Zeng, "Equalization for maximum likelihood detectors," *IEEE Trans. Magn.*, vol. 31, no. 2, pp. 1083–1088, Mar. 1995.

[20] R. Barry, A. Kavčić, S. W. LcLaughlin, A. Nayak, and W. Zeng, "Iterative timing recovery," *IEEE Signal Process. Mag.*, vol. 21, no. 1, pp. 89–102, Jan. 2004.